Indoor Wireless RF Energy Transfer for Powering Wireless Sensors

Hubregt J. VISSER

Holst Centre / imec, PO Box 8550, 5605 KN Eindhoven, The Netherlands

huib.visser@imec-nl.nl

Abstract. *For powering wireless sensors in buildings, rechargeable batteries may be used. These batteries will be recharged remotely by dedicated RF sources. Far-field RF energy transport is known to suffer from path loss and therefore the RF power available on the rectifying antenna or rectenna will be very low. As a consequence, the RF-to-DC conversion efficiency of the rectenna will also be very low. By optimizing not only the subsystems of a rectenna but also taking the propagation channel into account and using the channel information for adapting the transmit antenna radiation pattern, the RF energy transport efficiency will be improved. The rectenna optimization, channel modeling and design of a transmit antenna are discussed.*

Keywords

Antenna, channel, modeling, rectenna.

1. Introduction

Reducing energy consumption in (commercial) buildings will help in halting the climate change. Artificial lighting, for instance, contributes approximately 30% of electricity consumption in a commercial building, and buildings collectively account for 40% of the total world energy use [1]. By sensing people presence, temperature and light conditions, lighting and heating can be adjusted based on the readings. This so-called Smart Building Integration (SBI) concept relies on the widespread application of wireless sensors within a building.

A widespread introduction of wireless sensors and actuators will also contribute to a higher well-being of an aging population in an assisted living scenario, allowing the aged to live at home for a longer period.

Both aspects of SBI, sustainable energy and living in health, may be associated with a large economical drive. In 2007, the European home automation market earnings were estimated at €186.1 million and expected to reach €357.3 million in 2013 [2]. The European (retrofit) smart homes and assisted living market was in January 2010 expected to reach a size of €156.7 million in 2014 [3].

The widespread use of wireless sensors in offices and homes has been severely slowed down however, due to the costs of cabling. This is especially true for offices that are – on the average – reconfigured every five years [4]. To give an impression of these costs, cabling an average office unit or a four bed house is estimated at €7-11 thousand [5]. The use of battery powered sensors and actuators (sensing motion, presence, light, smoke and switching light, door bell, etc.) may cut these costs severely, up to 80% in offices [6]. The maintenance issues associated with battery powered sensors however, will not be tolerated by the market [7]. For every 50 battery-operated sensors, having a battery-life of one year, on average every week a sensor will be down which has to be found and the battery of this sensor needs to replaced and disposed of [8].

Energy harvesting may provide a solution to this maintenance problem. Possible sources for energy harvesting are vibration, ambient light, temperature gradients and ambient radio waves. The availability of energy harvesting sources of sufficient power cannot be guaranteed under all circumstances however.

A way of powering the wireless sensors is through employing rechargeable batteries that are being recharged by means of radio waves that are emitted by a dedicated source. This source is a Ultra High Frequency (UHF) or microwave transmitter that is placed in the vicinity of the sensors. Within this context we do not speak about RF energy harvesting but about RF energy transfer. Although transmitters are introduced, requiring energy, the general idea for SBI is to introduce some additional energy to save a multitude of this energy. This concept will only work if sensors can be powered at a sufficient distance from one dedicated transmitter that is subject to restricted transmit power levels [9]. This distance need to be in the range of two to five meters at minimum.

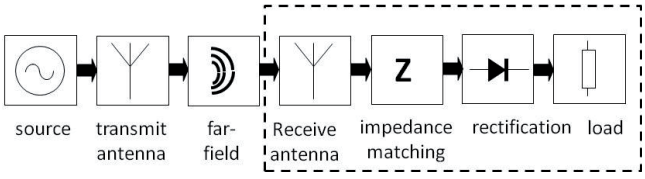

Fig. 1. Wireless RF power transmission system, with the rectenna in the dashed box.

The basis of an RF power transfer system, see Fig. 1, is an antenna connected to a rectifier. This rectifying antenna is commonly denoted rectenna. The rectenna converts the RF power incident on the antenna into usable DC power. This DC power will – in general, but not necessarily – pass through an Energy Storage System (ESS) before being delivered to the load.

By optimizing the rectenna, i.e. impedance matching the components of the rectenna, the conversion from incident RF power to DC power delivered to the load will be maximized. But next to optimizing the rectenna, Fig. 1 shows that also the propagation channel and the transmit antenna offer possibilities for increasing the overall RF power transfer efficiency.

In the following we will discuss the rectenna, the propagation channel and the transmit antenna, all subject to ongoing research at Holst Centre / imec.

2. Rectenna

As shown in Fig. 1, the main parts of a rectenna are the receiving antenna and the rectifying circuit. When an impedance matching network is being applied between the antenna and the rectifier, a standard 50Ω antenna may be applied. Our earlier work [10-12] has shown that it may be advantageous to directly match the antenna to the rectifying circuit. For a rectenna on a lossy FR4 PCB substrate this led to a more than 10% RF-to-DC power conversion efficiency improvement [10]. Not shown explicitly in Fig. 1 is a DC-to-DC voltage boost converter between the output of the rectifier and the load. If such a boost converter is applied, it needs to be impedance tuned to the output of the rectifying circuit. Consequently, the design of a rectenna starts with an analysis of the rectifying circuit.

2.1 Schottky Diode and Voltage Doubler

Since our rectifying circuits will consist of single or cascaded Schottky diodes, we need to be able to analyze such a diode. The equivalent circuit of a packaged Schottky diode is shown in Fig. 2.

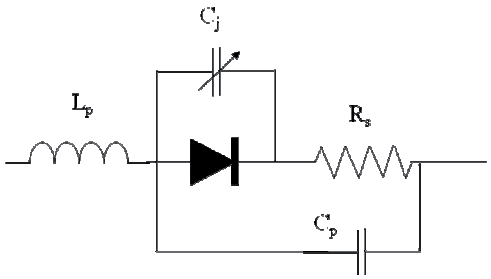

Fig. 2. Equivalent electrical circuit of a packaged diode.

In this equivalent circuit, the shown diode is an ideal one. C_j is the junction capacitance that is a function of the diode voltage, R_s is the bulk series resistance and L_p and C_p are the packaging parasitic inductance and capacitance, respectively. The values can be obtained from the diode's datasheet.

For determining the input impedance of this Schottky diode, a voltage generator V_g with internal resistor R_g is connected to left of the equivalent circuit and the right of the circuit is terminated in a parallel circuit of a capacitor C_L and a load resistor R_L. If $C_L \geq$ 0.1 µF [13], the load may be considered a short circuit in the frequency range 0.1 – 2.5 GHz for most commercially available Schottky diodes. For a short-circuit load the input impedance may be obtained in a very time-efficient way applying a Runge-Kutta (RK4) analysis [12], [13].

In Fig. 3, the thus calculated real and imaginary parts for a number of short-circuited Schottky diodes are shown as a function of input power at a frequency of 2.45 GHz. The correctness of the calculation method has been verified with measurements in [10], [12].

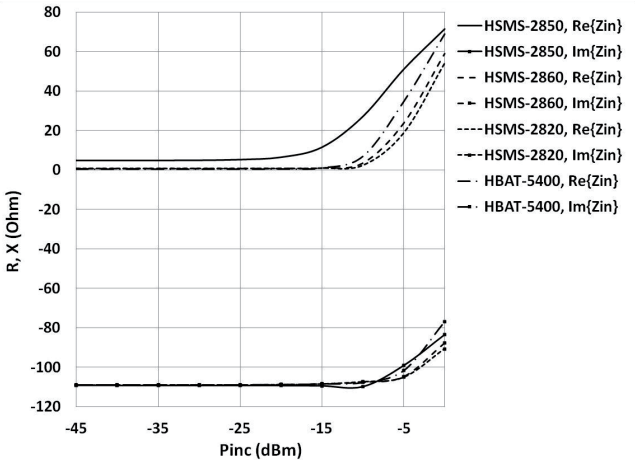

Fig. 3. Calculated real (top) and imaginary (bottom) values of the input impedance of a short-circuited, packaged Schottky diode as a function of available input power at 2.45 GHz. Diodes analyzed: Avago types HSMS-2850, HSMS-2860, HSMS-2820 and HBAT-5400.

The figure shows that for low input power levels, $P_{inc} <$ -15 dBm, the input impedance of all (short-circuited) diodes remain more or less constant. For battery charging and sensor powering applications we are more interested in the -15 dBm < P_{inc} < 0 dBm available input power range. There the impedance is highly dependent on the input power value.

If we design an antenna to be directly matched to the rectifier, we thus have to choose the anticipated available input power level carefully. To this end we define an impedance matching efficiency η_z as

$$\eta_z = 1 - |\Gamma|^2 \tag{1}$$

wherein Γ is the power wave reflection coefficient, defined by [14]

$$\Gamma = \frac{Z_L - Z_R^*}{Z_L + Z_R}. \tag{2}$$

In the above, Z_L is the input impedance of the rectifying circuit (here a single Schottky diode) and Z_R is the (complex) input impedance of the antenna. * denotes complex conjugate.

To demonstrate the importance of choosing the 'right' antenna impedance we show, in Fig. 4, the impedance matching efficiency as a function of available input power for two antenna input impedance values.

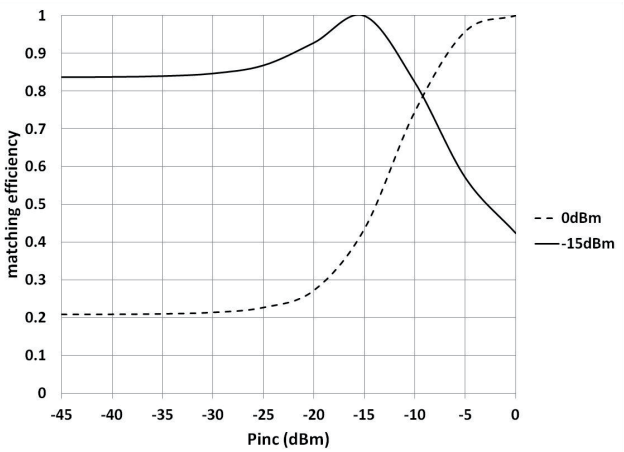

Fig. 4. Calculated impedance matching efficiency η_z for an Avago HSMS-2850 Schottky diode as a function of available input power. 0dBm (dashed line) indicates an antenna input impedance Z_R= (71 + j48) Ω, -15 dBm (solid line) indicates Z_R= (11 + j109) Ω, see Fig. 3.

The figure shows that for every input power level the antenna matching may be optimized, but it also shows that by carefully selecting an anticipated input power level a reasonable matching efficiency may be obtained for input power levels around this anticipated level.

For analyzing the DC behavior of the diode we cannot use the RK4 method. The RC-time of the load becomes orders of magnitude larger than the period of the source, resulting in the time-domain circuit equations becoming stiff [13]. Therefore we apply the implicit expression resulting from the Ritz-Galerkin method described in [15] for calculating the output voltage V_0 of a diode

$$\mathrm{I}_0\left(\frac{q}{nkT}\sqrt{8R_gP_{inc}}\right)=\left(1+\frac{V_0}{R_LI_s}\right)e^{\left(1+\frac{R_g+R_s}{R_L}\right)\frac{q}{nkT}V_0}. \quad (3)$$

In the above, I_0 is the zero-order modified Bessel function of the first kind, q is the electron charge, n is the diode's ideality factor, k is Boltzmann's constant, T is the temperature in Kelvin and I_s is the diode's saturation current. The other parameters have been defined already. n and I_s can be obtained from a diode's datasheet.

For the low input power levels we have to deal with, the DC output voltage of a single Schottky diode will be very low. Therefore, we will apply these diodes in a cascade. Most often we will use a cascade of two diodes, commonly known as a voltage doubling circuit, see Fig. 5.

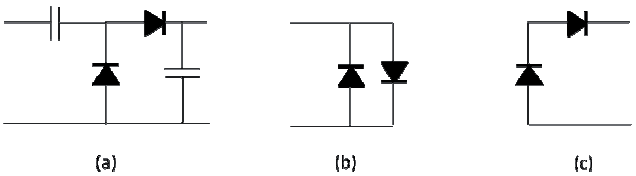

Fig. 5. Voltage doubling circuit. (a) Electrical circuit. (b) RF equivalent circuit. (c) DC equivalent circuit.

For the RF behavior, we may consider the capacitors to be short-circuits and from the equivalent circuit, see Fig. 5(b) we see that the input impedance is halved with respect to a single diode. For the DC behavior, we may consider the capacitors to be open-circuits and the two diodes will act as two in series connected voltage sources as shown in Fig. 5(c). For obtaining the RF input impedance, we apply the RK4 analysis of [10], [12] for a single short-circuited diode and half the obtained value. For obtaining the DC output voltage of the doubler, we apply equation (3) for a single diode as outlined in [16]: R_g is doubled and R_L is halved. Contrary to the procedure described in [16] we do not double the thus obtained output voltage, noticing that the approximate results match better with measurements in our region of interest for the input power, i.e. -15 dBm < P_{inc} < 0 dBm, see Fig. 6.

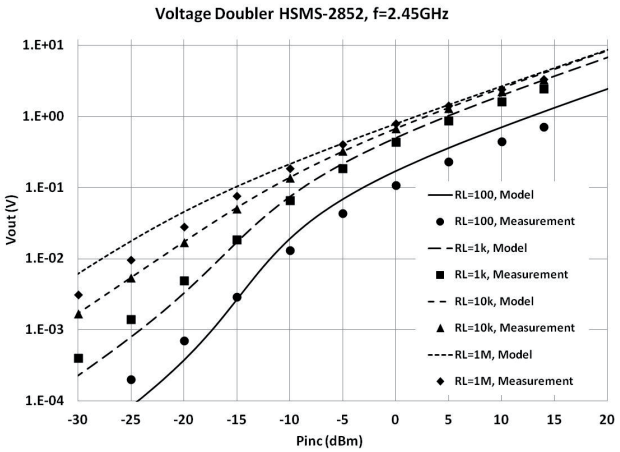

Fig. 6. Approximately calculated and measured output voltage of a voltage doubling circuit as a function of available input power. The voltage doubler is based on the Avago HSMS-2852 Schottky diode.

The DC output voltage as shown in the above figure has been calculated considering a 50Ω generator impedance. With the input impedance of the voltage doubling circuit now known (anti-parallel diode pair, see Fig. 5(b)), we can calculate the accepted power P_{acc} and, from the data in Fig. 6, obtain the RF-to-DC power conversion efficiency η_{con} as

$$\eta_{con}=\frac{V_0^2}{R_LP_{acc}}. \quad (4)$$

Fig. 7 shows the RF-to-DC power conversion efficiency of the (AVAGO HSMS-2852 based) voltage doubling circuit as a function of accepted power for several values of the load resistor.

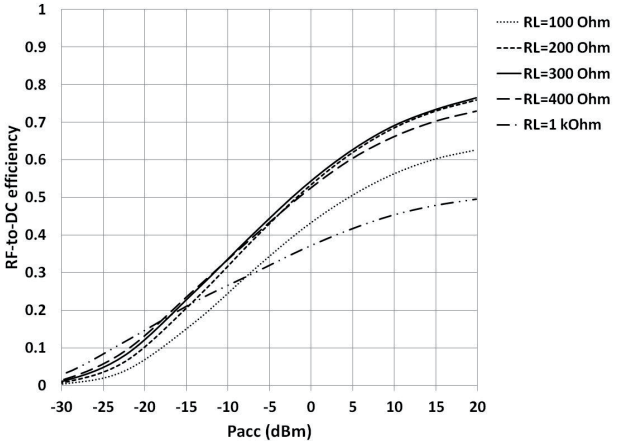

Fig. 7. RF-to-DC power conversion efficiency of a voltage doubler based on the Avago HSMS-2852 Schottky diode as a function of accepted input power for several load resistor values.

The figure shows that for this voltage doubling circuit in the power region of interest (15 dBm < P_{acc} < 0 dBm), a load resistance value between 300 and 400 Ω results in the highest RF-to-DC power conversion efficiency.

From Fig. 6 we see that the highest output voltage we can obtain in our input power region of interest is a few tenths of a Volt. This is not enough to charge a battery or to power a sensor. To realize a higher voltage we will need a DC-to-DC voltage converter.

2.2 DC-to-DC Voltage Converter

Not only will the output voltage of the rectifying circuit be too low for charging a battery, it will also change with a changing input power level. A DC-to-DC voltage converter will adapt the rectified voltage to a stable output voltage high enough for charging a rechargeable battery. The input impedance of this converter should be equal to the optimum load impedance value (300 – 400 Ω) of the rectifier circuit.

In [13], a discrete buck-boost converter is described. This converter can be used to charge a (not completely empty) battery within a voltage range of 2.1 to 4.5 V as long as the rectifier output voltage is between 0.21 and 1 V. The 0.21 V input under-voltage lockout is used to prevent the battery discharging due to an inefficient conversion. A battery over-voltage lockout is used to protect the battery from overcharging.

We define the DC-to-DC converter efficiency as

$$\eta_{DCDC} = \frac{P_{out}}{P_{acc}}. \tag{5}$$

This converter efficiency as a function of accepted input power, measured for three different batteries, is shown in Fig. 8.

We now have specified the most important efficiencies of the functional blocks that make up a rectenna, see Fig. 9.

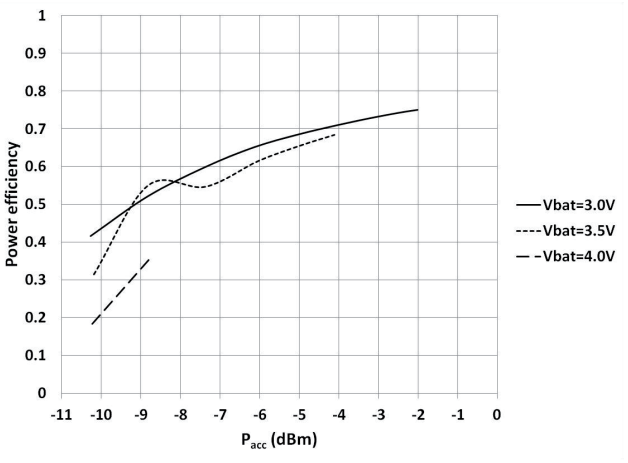

Fig. 8. Measured converter efficiency as a function of accepted power for three different batteries.

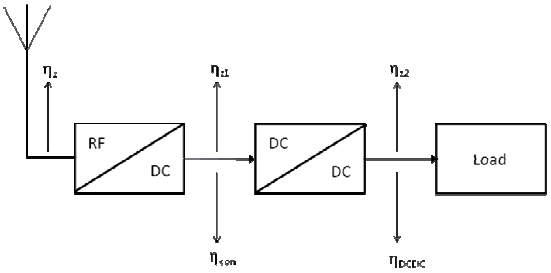

Fig. 9. Rectenna functional blocks and efficiencies.

The efficiencies η_z, η_{con} and η_{DCDC} have been discussed. The reflection efficiencies η_{z1} and η_{z2} are supposed to be unity for the discrete buck-boost converter discussed. The overall power efficiency of the rectennna is obtained by multiplying the individual block efficiencies. This means that for an antenna matched to an AVAGO HSMS-2852 based voltage doubler that is connected to our DC-to-DC voltage converter for charging a 3V battery with an incident power of 0 dBm, the total efficiency η_{tot} is given by $\eta_{tot} = \eta_{con} * \eta_{DCDC} = 0.55 * 0.8 = 0.44$, see Fig. 7 and 8.

The only component of the rectenna left to discuss is the antenna.

2.3 Antenna

In the previous sections we assumed that we have an antenna with the required complex input impedance. To design such an antenna, we start by selecting an antenna type that will be small enough to fit into the wireless sensor to be powered. Preferably the antenna will have enough geometrical dimensions that can be used to tune the antenna to the desired complex input impedance. A dedicated analysis model will help in obtaining an initial design in a time-efficient way [17]. A collection of approximate antenna analysis models may be found in [12].

Antennas that have been used successfully by the author are the rectangular microstrip patch antenna [10-13] and the strip folded dipole antenna [12], [13]. The microstrip antenna has been used for matching to an AVAGO

HSMS-2852 based voltage doubler for an input power of 0 dBm. This made an edge-feed of the rectangular patch feasible. For impedances associated with lower input power levels this needs not be true. A strip folded dipole antenna with a parasitic short-circuited dipole element, see Fig. 10, or a folded dipole with additional short-circuits in the arms [12] may then be employed to generate the desired input impedance.

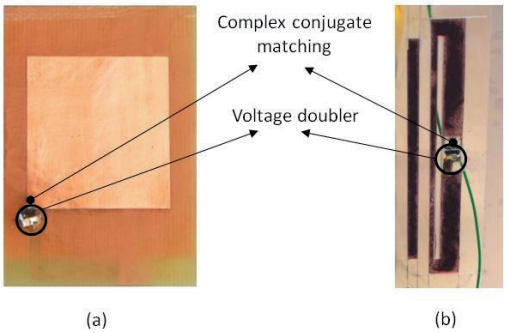

Fig. 10. Antennas for rectenna use. (a) Rectangular, edge-fed, microstrip patch antenna. (b) Strip folded dipole antenna with parasitic, short-circuited, dipole element.

2.4 System

A remote RF battery charger has been constructed, consisting of a rectangular microstrip patch antenna, directly impedance-matched to a HSMS-2852 based voltage doubler, see Fig. 10(a) and 11. The rectifier is connected to a discrete DC-to-DC voltage boost converter [13], see Fig. 11 and 12. The boost converter is connected to a 3V Li-Ion rechargeable battery, see Fig. 11. Next, the remote RF battery charger has been packaged to be used for powering a Commercially Of The Shelf (COTS) wireless sensor node. Fig. 13 shows the packaged 2.45GHz remote RF battery charger and a COTS 433MHz wireless temperature and humidity sensor.

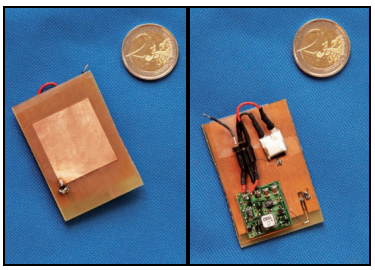

Fig. 11. System and components of a remote RF battery charger: (a) front view with rectangular microstrip patch antenna, (b) back view with microstrip antenna ground plane, discrete voltage boost converter and rechargeable battery.

The 433MHz wireless sensor measures and transmits temperature and humidity to a base station every 45 s. The sensor has been modified by removing the two AA 1.5 V batteries and bringing DC power lines outside the casing.

The value of the power needed for the 3V wireless sensor node has been obtained by measuring the supply current as a function of time for a constant voltage of 3 V. The current as a function of time is shown in Fig. 14. Fig. 15 shows one of the pulses in Fig. 14 in detail.

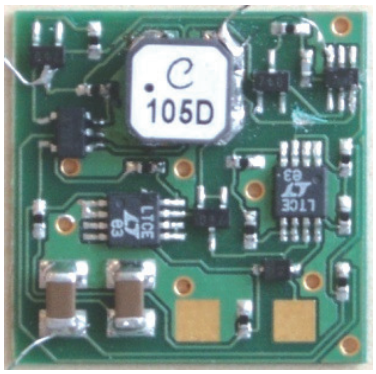

Fig. 12. PCB of DC-to-DC voltage (buck-boost) converter.

Fig. 13. Packaged 2.45GHz remote RF battery charger and COTS 433MHz wireless temperature and humidity sensor. 433MHz base station not shown.

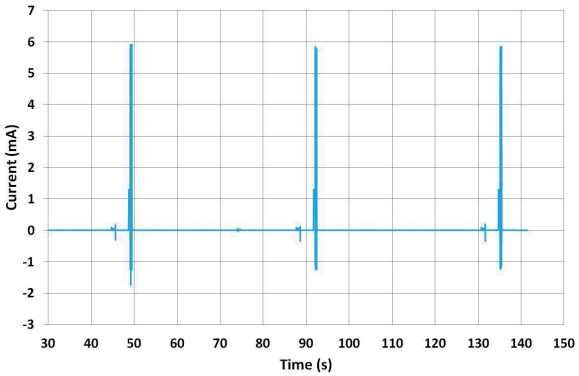

Fig. 14. Measured current as a function of time for a constant voltage of 3V for the COTS wireless sensor.

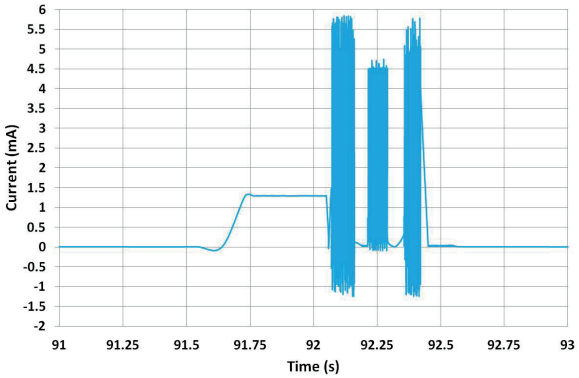

Fig. 15. Detail of the curve shown in Fig. 14.

Based on these measurements, the average power supply level needed is found to be 55 μW. The RF charger circuit itself, i.e. the boost converter, needs 17.9 μW.

3. Propagation Channel

The rectenna optimized for 0 dBm input power as described in the previous section has been used to measure the obtained DC power as a function of distance in an indoor Line of Sight (LoS) setup. In free space, radiated RF power will fall off as one over the square of the distance. In an indoor, reflective environment, the path loss may be described by an r^{-n} dependence, where r is the distance from the source. n may vary from 0.8 in a highly reflective environment [18] to 1.8 in a common office building [19-21]. In Fig. 16, the measured DC power as a function of distance from the source for two transmitting antennas is shown.

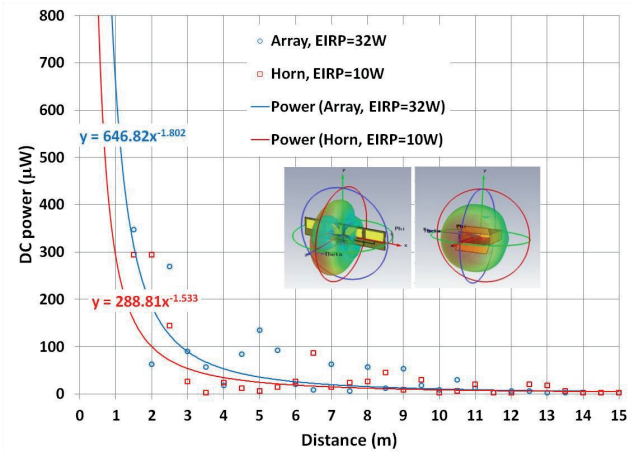

Fig. 16. Measured DC power from a rectenna in a LoS setup as function of distance. Frequency: 2.45 GHz. Transmitting and receiving antenna positioned 50 cm above the ground.

The measurements were conducted in a corridor with metal plating on the ceiling and doorposts made of metal. Also shown in the figure are the power trends through the measurement data. Even though the impedance matching efficiency, the RF-to-DC power conversion efficiency and the voltage converter efficiency decrease with decreasing input power, see Fig. 4, 7 and 8, we do observe a $n < 2$ behavior. We also see that a lower Effective Isotropic Radiated Power (EIRP), i.e. a wider transmit antenna pattern, leads to a higher DC power level at larger distances from the source. Obviously, through the mechanism of constructive interference of reflected waves the power level at the rectenna position may be optimized. What is needed then is a transmit antenna that can direct power directly to the rectenna and to the reflection points that result in in-phase contributions at the rectenna position. The radiation pattern should have 'nulls' in the directions that would result in anti-phase contributions, after reflection, at the rectenna position.

To assess these directions, a Geometrical Optics (GO) modeling of the surrounding is employed. Fig. 17 shows, as an example, how a second order, 2D reflection is constructed.

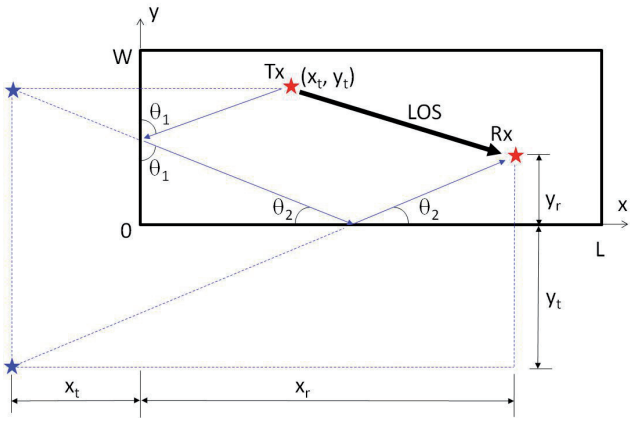

Fig. 17. Construction of a second order, 2D reflection.

Expanding this concept to the three dimensional surrounding finally gives for the received electric field $E_r(t)$

$$E_r(t) = \frac{\lambda}{4\pi} g_{0,1} \frac{E_t(t)}{d_{0,1}} e^{-j\frac{2\pi}{\lambda}d_{0,1}} + \sum_{m=1}^{R} \sum_{n=1}^{N(N-1)^{m-1}} \frac{\lambda}{4\pi} g_{m,n} \prod_{i=1}^{m} \left\{\rho_{i,n} e^{j\psi_{i,n}}\right\} \frac{E_t(t)}{d_{m,n}} e^{-j\frac{2\pi}{\lambda}d_{m,n}} \quad . \quad (6)$$

In the above, $E_t(t)$ is the transmitted electric field strength, $g_{m,n}$ is the product of the directivity functions of transmit and receive antennas in the directions of launched and received rays, respectively, $d_{m,n}$ is the total distance traveled by the n^{th} ray of order m, ρ is the reflection amplitude and ψ is the reflection phase. N is the number of reflecting surfaces and R is the number of reflections taken into account.

It suffices to take only the first couple of reflections into account to get a fair representation of the propagation in the surrounding. The corridor used for the measurements shown in Fig. 16 may be modeled as having PEC walls, floor and ceiling. The developed GO model has been verified by comparing the results with results obtained with *Savant* ray tracing software from *Delcross Technologies* [22], see Fig. 18.

The difference in Fig. 18 (a) for the GO and Savant simulation results is believed to be due to the fact that the antenna impedance changes due to the proximity of a wall are not taken into account in the GO model. Despite this discrepancy, the GO model is considered to be good enough to analyze the propagation channel and give directions for the transmit antenna design.

As an example, we show in Fig. 19 how a multi-beam antenna may increase the received power with respect to a single-beam antenna pointing at the receiver. The transmit antenna is pointing directly at the receive antenna and

also to the first order, constructive interference, reflection points in a PEC-cladded corridor.

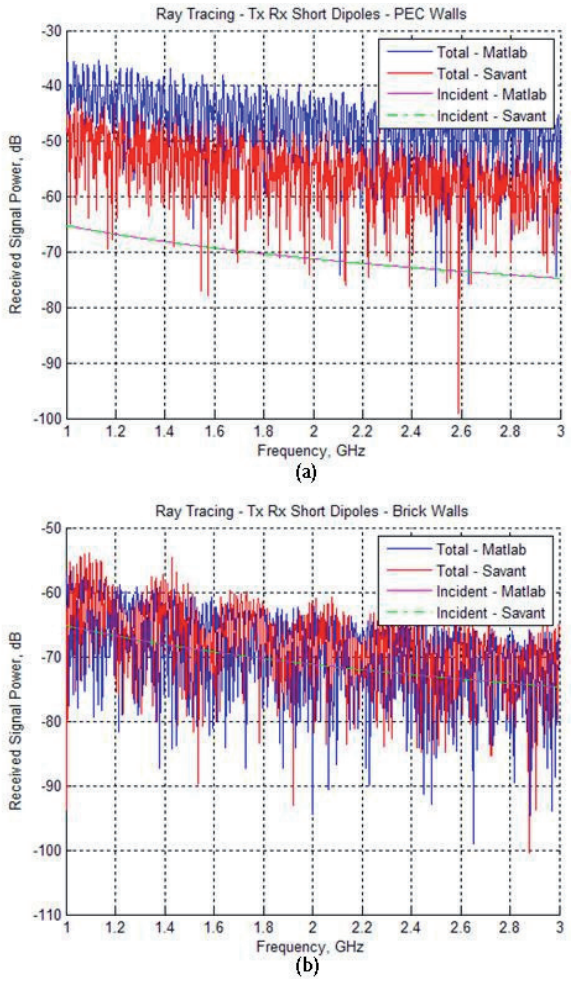

Fig. 18. Simulated received RF power in a LoS setup as a function of frequency. The surrounding is a box of 50m x 50m x 50m, having the origin at the centre. Tx and Rx antennas are short dipoles. The Tx antenna position is x = 12.5 m, y = -12.5 m, z = -12.5 m. The Rx antenna position is x = -12.5 m, y = 12.5 m, z = 12.5 m. (a) PEC walls. (b) Brick walls. The free space transmission (incident) is shown for reference.

Having thus shown the benefit of optimizing the transmit antenna radiation patter, the issue that remains is how to design such a transmit antenna.

4. Transmit Antenna

Since the transmit antenna beam shape depends on the environment and the position of the receivers in this environment, we need a transmit antenna with beam-shaping capabilities. A phased array solution in which the array element phases or phases and amplitudes can be manipulated will be too costly for SBI. A good alternative is provided by a switched array antenna [23], in which one dipole/monopole element will be driven and parasitic dipoles/monopoles will be switched open or short-circuited/grounded. Instead of directly designing a three-dimensional switched array antenna, we will start with a two-dimensional switched array antenna for beam-shaping capabilities in the horizontal plane.

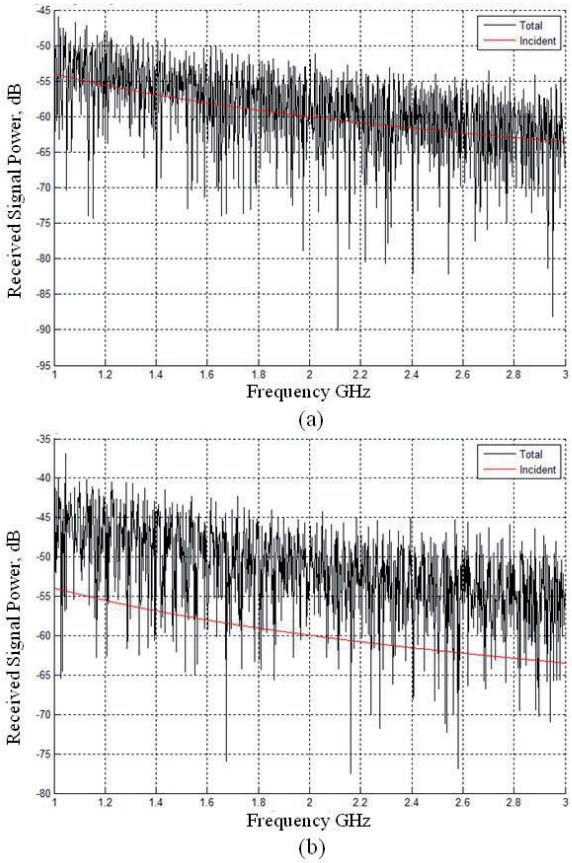

Fig. 19. Simulated received RF power in a LoS setup as a function of frequency. The surrounding is a box of 50m x 50m x 50m, having the origin at the centre. The Tx antenna is a multi-beam antenna, the Rx antenna is an omni-directional antenna. The Tx antenna position is x = 12.5 m, y = -12.5 m, z = -12.5 m. The Rx antenna position is x = -12.5 m, y = 12.5 m, z = 12.5 m. (a) Single-beam antenna. (b) Multi-beam antenna. The free space transmission (incident) is shown for reference.

To create more gain than with the 'standard' switched array antenna as shown in e.g. [23], we have extended the concept to include Yagi-Uda linear array antennas. The Yagi-Uda linear array antennas are angularly displaced, sharing a centrally placed active element. The top view of a seven Yagi-Uda switched array configuration is shown in Fig. 20. The Yagi-Uda arrays each consist of five elements, one active element, one reflector and three directors, see Fig. 21.

Fig. 20 shows that by 'switching on' additional elements, next to the reflectors and directors of selected Yagi-Uda linear arrays, parabolic-like reflectors can be created, thus enhancing the radiation. This enhancement consists of decreasing the back- and side-lobe levels of the radiation pattern.

The modeling of the antenna is based on the model described in [24] for thin wire dipoles. The model has been improved by first replacing the self-impedance with the

'three-term' model of King [25], [26] for thick dipole antennas. Next, for a higher accuracy, the thin wire mutual coupling expressions have been replaced by a thick wire mutual coupling analysis based on [27]. The details of the analysis may be found in [28]. With the impedances known, the currents on the driven and 'switched on' elements can be determined. Integration of these currents over the active dipole elements results in the radiation pattern of the antenna [24]. The open-circuited parasitic elements are considered to carry no current and thus being electromagnetically invisible.

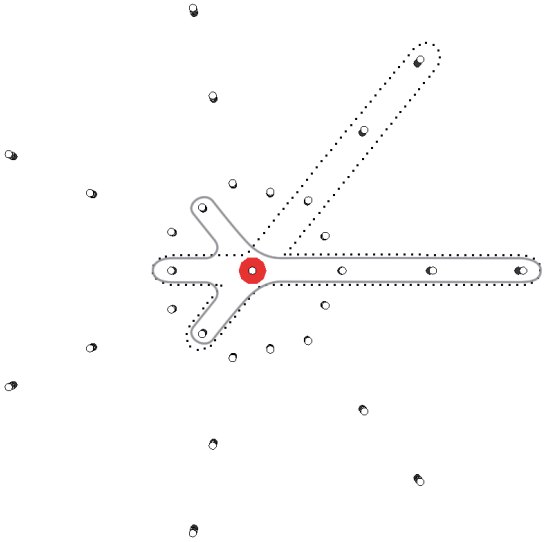

Fig. 20. Top view of a seven, 5-element switched Yagi-Uda array antenna.

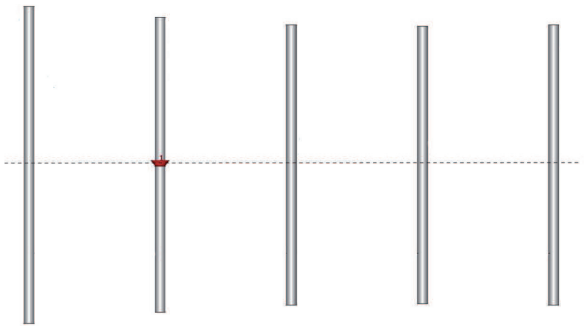

Fig. 21. Five-elements Yagi-Uda linear dipole array antenna.

The switching elements will be PIN diodes. These PIN diodes will be incorporated into the model by virtue of their equivalent electrical circuits, see Fig. 22.

The choice for a particular PIN diode will be based on the R_s resistance value (as low as possible) and the resonance frequency that must be sufficiently removed from the antenna operating frequency. The mere effect of the PIN diodes will then be a small lowering of the transmit antenna gain.

The approximate analysis method is sufficiently fast when implemented in software to allow for an automatic design by incorporating it into a Genetic Algorithm optimization shell. The constraints of the optimization are the radiation pattern, in particular the gain, front to back ratio and the side lobe level as well as the impedance matching. Designs have been used as input in a full wave analysis program (CST Microwave Studio®) for verification purposes. Radiation pattern analysis results are shown in Fig. 23.

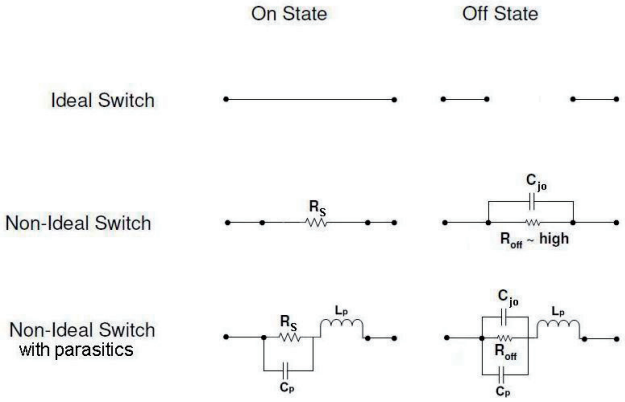

Fig. 22. Equivalent electrical circuit models for PIN diode switch.

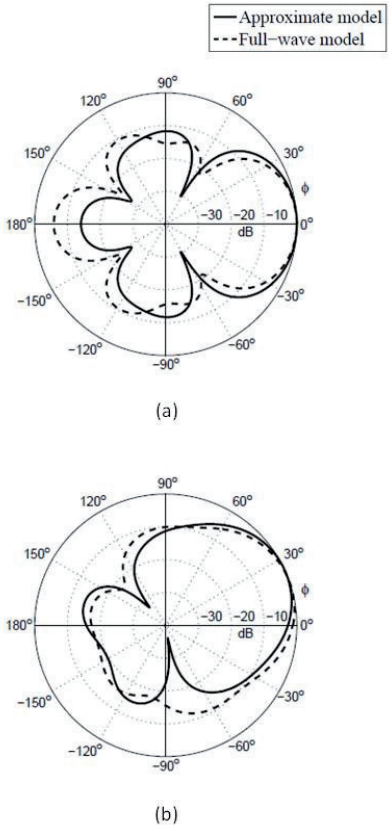

Fig. 23. Approximate and full-wave normalized radiation pattern simulation results for a switched array antenna consisting of seven Yagi-Uda linear array antennas. (a) Beam steered to $\varphi=0^0$. (b) Beam steered to$\varphi=30^0$.

As a final verification, an antenna should be fabricated and characterized. The 2.45GHz antenna design for which the simulated radiation patterns have been shown in

Fig. 23 would be the ideal choice. However, we found that the anechoic chamber to be used for reflection and radiation pattern measurements was not shielded and strong WiFi interference signals were present from nearby and further removed locations. The nearby interferer could be switched off. Unfortunately we did not have access to the other source of interference. Therefore we decided to design and realize a prototype switched dipole antenna operating on 868 MHz. Instead of using switches, we applied interchangeable open- or short circuited parasitic elements. Furthermore, we used strips instead of cylindrical dipoles for the ease of construction, see Fig. 24.

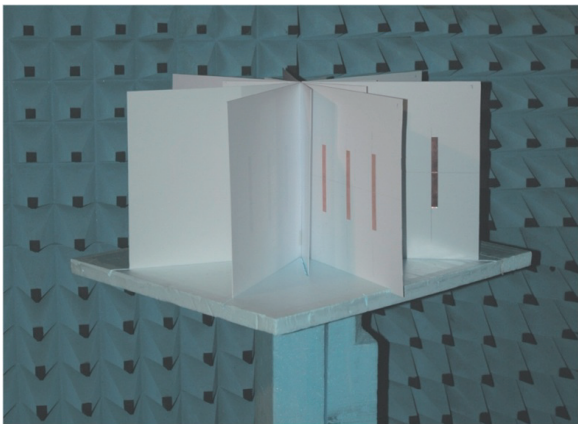

Fig. 24. Realized 868MHz, seven strip Yagi-Uda switched array antenna in anechoic chamber.

The strip width w is 1.25 cm. The element heights h_1, h_2, h_3, h_4 and h_5 are 6.70 cm, 7.91 cm, 6.46 cm, 6.45 cm and 6.90 cm, respectively, where 1 is the driven element, 2 is the reflector and 3, 4 and 5 are the directors the last one being the outer one. The inter-element distances d_{12}, d_{31}, d_{34} and d_{45} are 6.89 cm, 7.34 cm, 7.34 cm and 7.34 cm respectively. The strips are placed on sheets of 1mm thick High Impact Polystyrene (HIPS). The relative permittivity of this material has been determined to be 2.8.

In Fig. 25 we show the simulated and measured reflection coefficient as a function of frequency.

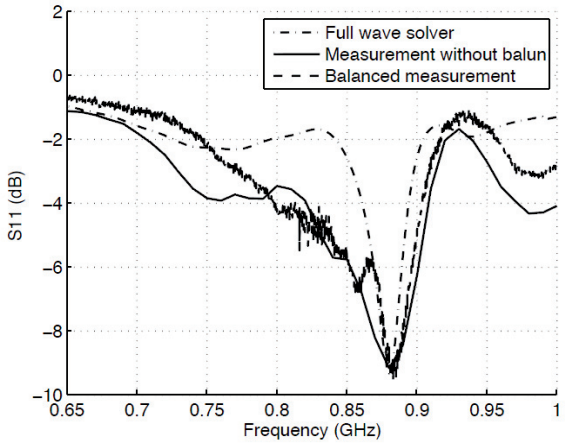

Fig. 25. Simulated and measured reflection coefficient as a function of frequency for the switched array antenna shown in Fig. 24.

The figure shows a reasonable to fair agreement between simulation and measurement results. Moreover it demonstrates that for this antenna cable currents do not play an important role.

Simulated and measured representative radiation patterns are shown in Fig. 26.

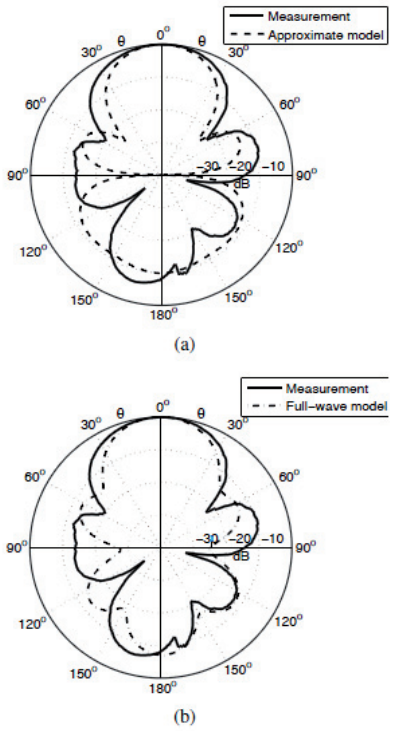

Fig. 26. Normalized E-plane radiation pattern for the antenna shown in Fig. 24. (a) Measurement vs. approximate model. (b) Measurement vs. full-wave model.

5. Future Work

For a practical implementation of the switched Yagi-Uda array antennas we need to transform the dipole design into a monopole design with a finite ground plane. To overcome the beam elevation effect of a finite planar ground plane, we will apply a so-called skirted ground plane. The concept of such an antenna, as well as a simulated radiation pattern, is shown in Fig. 27. Fig. 28 shows a first realized prototype antenna.

Then the whole system should be implemented, tested and calibrated.

6. Conclusions

RF energy transport suffers from path loss. Therefore the RF power available on a rectenna will in general be very low. As a consequence, the RF-to-DC conversion efficiency will also be very low. This means that special care must be taken in improving the impedance matching efficiency between the various subsystems of a rectenna,

i.e. the antenna-rectifier, rectifier-converter and converter-load connections. Furthermore, the boost converter efficiency needs to be maximized.

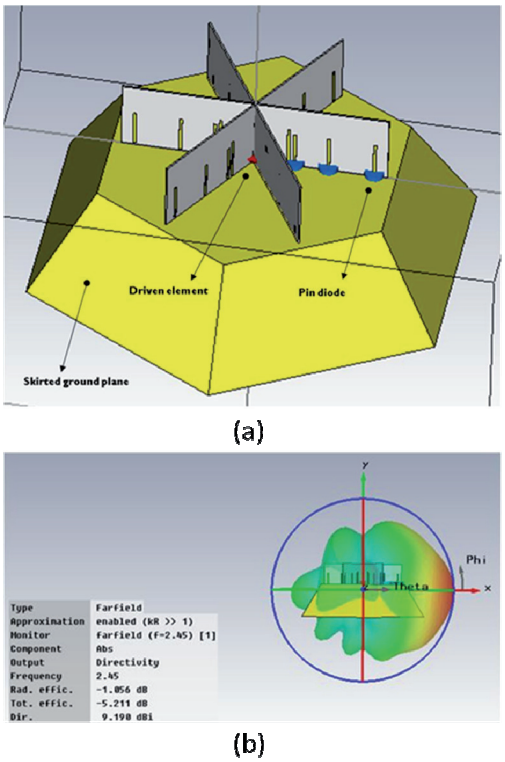

Fig. 27. Switched monopole Yagi-Uda Array antenna. (a) Array antenna consisting of six Yagi-Uda array antennas on a skirted, finite ground plane. (b) Simulated radiation pattern of the array with one Yagi-Uda array switched on.

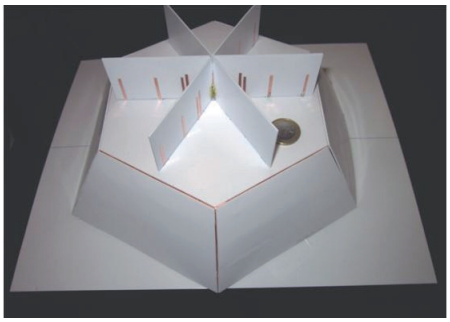

Fig. 28. Prototype of the antenna shown in Fig. 27(a).

Next to these rectenna optimization measures, the input power of the rectenna should be maximized without increasing the transmitter EIRP. This may be accomplished by adapting the transmitting antenna radiation pattern to the propagation channel characteristics.

Acknowledgements

The author would like to thank Matt Miller from Delcross Technologies [22] for providing access to the Savant software. Furthermore he thanks his (former) students Irina Paraschiv, Amanuel Kihshen and Stefan Lem.

References

[1] Intelligent buildings – A holistic perspective on energy management. *Electrical Review*, October 2009. Available at: http://www.electricalreview.co.uk/features/118645.

[2] European home automation market is set to double. *Business Wire*, August 2007. Available at: http://wwwallbusiness.com/services/business-services/4551021-1.html.

[3] European smart homes and ASSISTED living – Advanced technologies and global market (2009-2014). *Markets and Markets*, January 2010. Available at: http://marketsandmarkets.wordpress.com/2010/01/21/.

[4] DUGRE, M., FREYER, F., ANDERS, A. Bacnet and EnOCean enable energy efficient buildings. *Bacnet and EnOcean White Paper*. Available at: http://www.enocean-alliance.org /fileadmin /redaktion/enocean-alliance/pdf/whitepaper_BACNET_EnOcean_en.pdf.

[5] LANDOW, N. Wiring a building. *Macktez*, February 2004. Available at: http://www.macktez.com/recommendators/00826.html.

[6] HIRAI, J., KIM, T., KAWAMURA, A. Wireless transmission of power and information for cableless linear motor drive. *IEEE Transactions on Power Electronics*, 2000, vol. 15, no. 1, p. 21 to 27.

[7] Energy harvesting, wireless and next generation energy. *Ivory Egg*, March 2009. Available at: http://www.ivoryegg.co.uk/tag/energy-harvesting/.

[8] LINKS, C. The third wireless revolution – sensor networks. *Greenpeak Technologies*, June 2009. Available at: http://www.greenpeak.com/Company/Opinions/CeesLinksColumn02.pdf.

[9] European Radiocommunications Committee, ERC Recommendation 70-03 Relating to the Use of Short Range Devices (SRD), *ERC/REC 70-03*, 2009.

[10] THEEUWES, J., VISSER, H., VAN BEURDEN, M., DOODEMAN, G. Efficient, compact, wireless battery design. In *Proceedings of the European Microwave Conference*. Munich (Germany), 2007, p. 991 – 994.

[11] VISSER, H. THEEUWES, J., VAN BEURDEN, M., DOODEMAN, G. High-efficiency RF-rectenna design. *EDN*, 2007, vol. 52, no. 14, p. 34.

[12] VISSER, H. *Approximate Antenna Analysis for CAD*. Chichester: John Wiley & Sons, 2009.

[13] VISSER, H., POP, V. OP HET VELD, B., VULLERS, R. Remote RF battery charging. In *Proceedings of PowerMEMS*. Leuven (Belgium), 2010, 4 p.

[14] RAHOLA, J. Power waves and conjugate matching. *IEEE Transactions on Circuits and Systems II: Express Briefs*, 2008, vol. 55, no. 1, p. 92 - 96.

[15] HARRISON, R., LE POLOZEC, X. Nonsquarelaw behavior of diode detectors analyzed by the Ritz-Galerkin method. *IEEE Transactions on Microwave Theory and Techniques*, 1994, vol. 42, no. 5, p. 840-846.

[16] Agilent Technologies, Designing the virtual battery. *Application Note 1088*, 1994.

[17] VISSER, H., VULLERS, R. Automatic antenna design for wireless energy harvesting. In *Proceedings of Loughborough Antennas and Propagation conference.* Loughborough (UK), 2010, 4p.

[18] HWU, S., LOH, Y., SHAM, C. Propagation characteristics of international space station wireless local area network. In *Proceedings Radio and Wireless Conference*. 2004, p. 407 – 410.

[19] PHAIBOON, S., PHOKHARATKUL, P., SOMKUARNPARIT, S., BOONPIYATHUD, S. Upper- and lower-bound path-loss modeling for indoor line-of-sight environments. In *Proceedings Asia-Pacific Microwave Conference APMC2005*. 2005, 4p.

[20] DUANGSUWAN, S., LENKACHORN, T., CHINSAWATPAND, S., PRONGWANG, S. Experimental study of polarimetric measurement of RFID transfer function within an indoor environment. In *Proceedings IEEE Malaysia International Conference on Communications*. 2009, p. 686 – 690.

[21] MOLKAR, D. Review on radio propagation into and within buildings. *IEE Proceedings – H*, 1991, vol. 138, no. 1, p. 61 – 73.

[22] Available at: http://www.delcross.com/products-savant.php.

[23] SCHLUB, R., THIEL, D. Switched parasitic antenna on a finite ground plane with conductive sheet. *IEEE Transactions on Antennas and Propagation*, 2004, vol. 52, no. 5, p. 1343 – 1347.

[24] VISSER, H. *Array and Phased Array Antenna Basics*. Chichester: John Wiley & Sons, 2005.

[25] KING, R., WU, T. The imperfectly conducting cylindrical transmitting antenna, *IEEE Transactions on Antennas and Propagation*, 1966, vol. 14, p. 524 – 534.

[26] KING, R., HARRISON, C., ARONSON, E. The imperfectly conducting cylindrical transmitting antenna: Numerical results. *IEEE Transactions on Antennas and Propagation*, 1966, vol. 14, p. 535 – 542.

[27] KING, R. *Cylindrical Antennas and Arrays*. Cambridge, University Press, 2002.

[28] PARASCHIV, I., VISSER, H. Analysis of coupling between thick dipoles within antenna arrays. In *Proceedings of the European Microwave Conference*. Amsterdam (The Netherlands), 2012.

About Authors ...

Hubregt VISSER was born in Goes, The Netherlands in 1964. He received his M.Sc. from Eindhoven University of Technology, The Netherlands, in 1989 and his Ph.D. from Eindhoven University of Technology and Leuven Catholic University, Belgium, in 2009. His research interests include full-wave and approximate modeling of small antennas, rectennas and array antennas. He is the author of 'Array and Phased Array Antenna Basics' (Wiley, 2005), Approximate Antenna Analysis for CAD' (Wiley, 2009) and 'Antenna Theory and Applications' (Wiley, 2012).